Site symmetry in binary and ternary tin silicate glasses—^{29}Si and ^{119}Sn nuclear magnetic resonance

2003 J. Phys.: Condens. Matter 15 S2457

(http://iopscience.iop.org/0953-8984/15/31/320)

INSTITUTE OF PHYSICS PUBLISHING JOURNAL OF PHYSICS: CONDENSED MATTER

J. Phys.: Condens. Matter **15** (2003) S2457–S2472 PII: S0953-8984(03)65166-0

Site symmetry in binary and ternary tin silicate glasses—^{29}Si and ^{119}Sn nuclear magnetic resonance

D Holland[1,4], A P Howes[1], R Dupree[1], J A Johnson[2] and C E Johnson[3]

[1] Department of Physics, University of Warwick, Coventry CV4 7AL, UK
[2] Materials Science Division, Argonne National Laboratory, Argonne, IL 60439, USA
[3] Physics Department, Northern Illinois University, DeKalb, IL 60115, USA

E-mail: d.holland@warwick.ac.uk

Received 24 June 2003
Published 23 July 2003
Online at stacks.iop.org/JPhysCM/15/S2457

Abstract

^{29}Si and ^{119}Sn nuclear magnetic resonance (NMR) spectroscopy has been performed on binary xSnO$(100-x)$SiO$_2$ and ternary xR$_2$O$(50-x)$SnO50SiO$_2$ glasses (R = Li, Na, K, Rb for the ^{29}Si NMR and R = Na for ^{119}Sn NMR). The spectra obtained have been fitted to obtain the spectral parameters. The variation of these parameters as a function of composition has been compared with structural information from previous density, neutron diffraction and Mössbauer spectroscopy studies. Tin is found to be present as Sn(II) in the binary silicate glasses but some Sn(IV) is present in the ternary glasses. The fraction of tin in the Sn(IV) oxidation state increases with the concentration of Na_2O. The ^{29}Si chemical shift reflects the average oxygen coordination number in the glass and the electronegativity of the neighbouring species. The ^{119}Sn chemical shift shows different behaviour with SnO concentration for the binary and ternary systems and the latter give significantly narrower lines, indicating more symmetric ^{119}Sn sites.

1. Introduction

There are several main-group heavy metals of electronic structure ns^2np^m which exhibit two oxidation states, $+m$ and $+(m+2)$. For the heavier elements (Tl, Pb, Bi) the lower oxidation state is the more stable, whilst for the preceding row (In, Sn, Sb, Te) the higher oxidation state is initially more stable but is replaced by the lower oxidation state with increasing nuclear charge. The non-bonding 'lone pair' of electrons occupies the spherically symmetric ns orbital in the gas phase ion M^{m+} but in the condensed state it occupies s–p or s–p–d hybridized orbitals and assumes steric importance in the crystal structures adopted. This is clearly seen in the metal oxides. In PbO and SnO there are 5 sp^3d hybrid orbitals, one occupied by the lone pair

[4] Author to whom any correspondence should be addressed.

at the apex of a square pyramid and the others bonded to oxygen atoms to form the base of the pyramid. In Sb_2O_3, trigonal pyramids are formed based on four sp^3 hybrids with once more a lone pair occupying one apex of the roughly tetrahedral distribution of orbitals. In TeO_2 the sp^3d hybrids form distorted trigonal bipyramids with the lone pair occupying one of the equatorial positions. A notable feature of these oxides is that they can all be important constituents of glasses, ranging from the modifier Tl_2O to the conditional glass formers TeO_2 and Sb_2O_3. We are studying glasses containing these oxides, using a variety of techniques, to determine how the lone pair of electrons participates in the symmetry of the environment of the metal cations. In this paper we report nuclear magnetic resonance (NMR) spectroscopy studies of binary and ternary silicate glasses containing SnO. Comparison is made with information obtained using Mössbauer spectroscopy, with particular emphasis on how the symmetry of the Sn(II) environment is influenced by glass composition and the charge distribution in the lone-pair orbital. Previous work [1–3] demonstrated that Sn(II) in these glasses adopts a pseudotetrahedral sp^3 arrangement of orbitals where one orbital is occupied by the electron lone pair. This is quite different from the bonding observed in the pure crystalline oxides, but is more like that observed in oxide compounds. The asymmetry of this arrangement was confirmed by the large quadrupole splitting of the ^{119}Sn Mössbauer resonance from these samples [2, 3].

2. Experimental details

2.1. Sample preparation

Glasses in these series were prepared [2, 4] by the route first described by Keysselitz and Kohlmeyer [5] and later used by Carbo-Nover and Williamson [6]. The systems consisted of the binary tin silicate $x\mathrm{SnO}(100-x)\mathrm{SiO}_2$ $20 \leqslant x \leqslant 80$ and several series of ternary glasses, based on the 50 mol% SnO binary, with the nominal formula $x\mathrm{R}_2\mathrm{O}(50-x)\mathrm{SnO}50\mathrm{SiO}_2$. 0.1 mol% of Fe_2O_3 was also added to each glass batch to reduce the ^{29}Si and ^{119}Sn relaxation times. The required stoichiometric proportions of starting materials (stannous oxalate SnC_2O_4 plus SiO_2 and R_2CO_3, where R is Li, Na, K or Rb) were calculated to give a 50 g batch and the powders were mixed and pressed into pellets which were packed into a silica crucible. This was placed under another inverted crucible and heated at 10 °C min^{-1} to 1000–1200 °C (depending on composition) where it was held for 48 min before being removed from the furnace to cool in air. Since Sn(II) is thermodynamically unstable with respect to Sn(IV), some conversion can occur during melting by either oxidation or disproportionation. Disproportionation was observed in these systems, with metallic tin sinking to the bottom of the melt and SnO_2 rising to the surface. This surface crust was removed mechanically and the remaining glass was separated from the crucible and metallic tin deposits and then stored in a desiccator until required for subsequent experiments. Disproportionation means that the glasses are generally of lower SnO content than the nominal composition. This effect is strongly dependent on the glass melting temperature and is therefore less of a problem for glasses with high alkali content. The compositions of these glasses were obtained by chemical analysis (Pilkington plc) with the exception of the sodium tin silicate glasses used for the NMR experiments.

2.2. Glass characterization

X-ray diffraction was performed on powdered material to check for amorphousness and the densities of bulk glasses were determined by Archimedes' principle with distilled water or 1,1,1-trichloroethane as the immersion fluid [4].

2.3. Neutron diffraction

Neutron diffraction measurements were carried out using either GLAD (the Glass, Liquids and Amorphous Materials Diffractometer) at IPNS (the Intense Pulsed Neutron Source) at the Argonne National Laboratory or LAD (the Liquid and Amorphous Diffractometer) at ISIS at the Rutherford Appleton Laboratory. Details have been published elsewhere [1, 3]. Total real space correlation functions $T(r)$ were evaluated by Fourier transformation with a Lorch modification function used to reduce termination effects associated with the cut-off at Q max.

2.4. Mössbauer spectroscopy

Mössbauer spectra were obtained [2, 3] at the Department of Physics, Liverpool University, in standard transmission mode, under a constant acceleration regime, with a solid state germanium detector. The source (Ca $^{119}SnO_3$—linewidth 0.9 mm s^{-1}) was at room temperature and the absorber at 77 K. Calibration was performed against an ^{57}Fe foil at room temperature.

2.5. Nuclear magnetic resonance (NMR)

^{29}Si magic angle spinning (MAS) NMR spectra were obtained on a CMX360 spectrometer, at a frequency of 71.54 MHz, using a Chemagnetics probe with a 6 mm rotor and speed of 3 kHz. The pulse length was 2 μs ($<\pi/2$) and a delay of 5 s was found to be sufficient to avoid saturation in the iron-doped samples. Typically 7000 acquisitions were made for each spectrum and 100 Hz of line broadening were applied prior to Fourier transformation of the free induction decay (FID). The spectra were referenced to tetramethylsilane (TMS).

^{119}Sn static NMR was performed at 88.75 MHz on a CMX240 spectrometer using a 9.5 mm probe. A 90–τ–180 echo sequence was used with the 90° pulse being 1.5 μs and τ being 50 μs. The T_1s for the glasses were typically 85 s for undoped samples and 5 s for samples doped with 0.1 mol% Fe_2O_3. For the latter, a recycle delay of 20 s was used and typically 2000 acquisitions were made. Prior to Fourier transformation, 4 kHz of line broadening was applied. Only static spectra are presented since spinning at 11 kHz failed to narrow the lines. The spectra were referenced to aqueous $SnCl_2$ solutions which were freshly prepared each time.

3. Results

3.1. Glass characterization

All the glasses were free of crystalline material. The nominal and analysed compositions are listed in table 1 along with the measured densities and calculated molar volumes [4]. The latter are plotted against SnO concentration in figure 1.

3.2. Neutron diffraction

The detailed results for the binaries [1] and ternaries [3] are reported elsewhere. Figure 2 shows the distinct scattering plots for the binary samples in comparison with a partially crystalline sample. This illustrates a characteristic of these SnO-containing glasses, that there exist intermediate range features based on the retention of the well-defined [SnO_3] polyhedron. This is shown by the development, with increasing SnO content, of intermediate range order (IRO) peaks at ∼1 and ∼2.1 $Å^{-1}$, which eventually coincide with the features produced by the crystalline material. The neutron diffraction total correlation function $T(r)$ was used to provide geometric information, namely interatomic distances and bond angles.

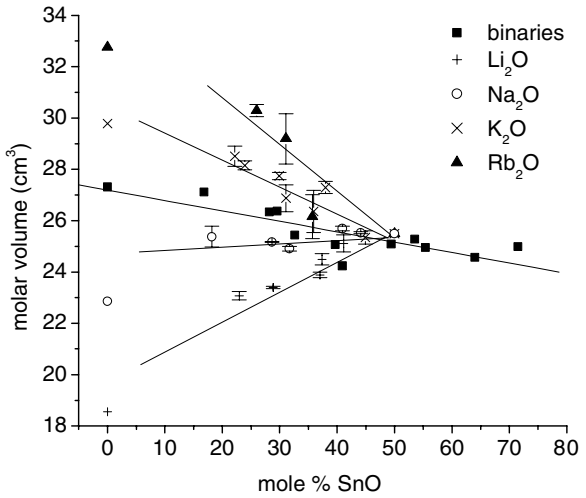

Figure 1. Molar volume of the glasses as a function of SnO content and alkali type. The values at zero SnO content are those for pure SiO_2 and the alkali metal metasilicate glasses R_2SiO_3.

Table 1. Nominal and analysed compositions (mol%) of the xSnO$(100-x)$SiO$_2$ binary and the xR$_2$O$(50-x)$SnO50SiO$_2$ ternary glasses. The error on the analysed values is typically 1 mol% or less. Each glass contained an additional 0.1 mol% Fe_2O_3 to reduce the ^{29}Si and ^{119}Sn relaxation times. Values of molar volume have an associated error of 0.2 cm^3 mol^{-1} but could be as high as 1.

SnO nominal	SnO	SnO_2	SiO_2	Li_2O	Na_2O	K_2O	Rb_2O	Molar volume (cm^3 mol^{-1})
30	32		68					28.0
40	37		63					26.1
50	47		53					25.5
60	53	3	44					25.3
45	41		55	4				25.1
40	37		54	9				24.5
30	29		54	17				23.4
25	23	2	55	21				23.1
45	41		53		6			25.7
37.5	32		56		13			24.9
30	29		50		21			25.2
20	18	3	53		26			25.4
45	36	1	58			5		26.4
40	31	1	58			10		26.9
30	24		56			20		28.1
45	36		59				5	26.1
35	32		56				12	29.2
30	26		56				18	30.3

O–Sn–O bond angles θ were obtained from the Sn–O and O–O distances ($\sin(\frac{\theta}{2}) = \frac{R_{O-O}}{2R_{Sn-O}}$). R_{Sn-O} can be determined quite accurately but there is greater uncertainty about R_{O-O} since the O–O peak is often overlaid with other correlations. The neutron diffraction data confirmed that the coordination number of tin to oxygen is 3.

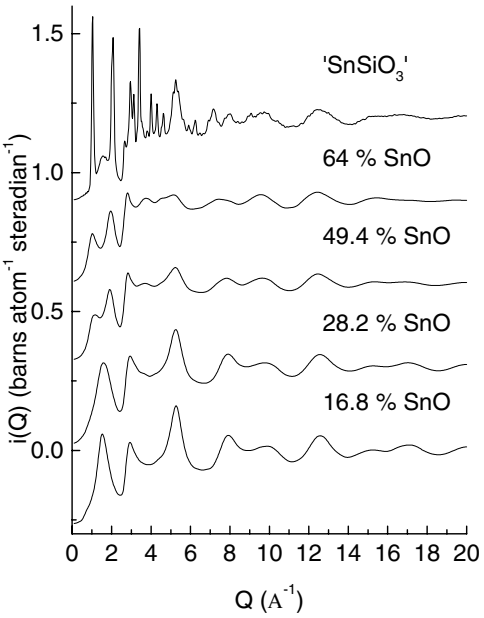

Figure 2. Distinct scattering versus Q for the binary glasses and a partially crystallized sample. The crystal phase is known not to be $SnSiO_3$ but this is the JCPDS assignment.

3.3. Mössbauer spectroscopy

A typical ^{119}Sn Mössbauer spectrum is shown in figure 3 to illustrate the parameters reported previously [2, 3] which will be discussed in comparison with the NMR data. These parameters are the isomer shift δ (w.r.t. SnO_2) and the quadrupole splitting Δ (both in mm s^{-1}). The spectrum is typical of a single Sn(II) site but the quadrupole split line is broadened by the range of site distortions present in a glass. The very large quadrupole splitting shows that Sn(II) is in a very asymmetric environment due to the presence of the lone pair of electrons. In some samples a small feature at $\sim$0 mm s^{-1} indicates the presence of some Sn(IV). Since this has a closed shell electron configuration, and is typically octahedrally coordinated, the quadrupole splitting is not resolvable. Figure 4 shows how the Mössbauer shift and quadrupole splitting vary with SnO content.

3.4. Nuclear magnetic resonance

^{29}Si. Figure 5 shows a typical spectrum in which a central asymmetric resonance can be seen; this is the isotropic peak, with a spinning sideband to each side of that peak. Whilst it is possible to fit the central peak with two Gaussians in the case of the binary glasses, the resolution is insufficient in the case of the ternaries where Si can have Si, Sn and R as possible next nearest neighbours. To assess the impact of composition on the Si environment, we have therefore considered peak shift alone and the variation of this with SnO content is shown in figure 6.

^{119}Sn. Figures 7(a) and 8(a) show some of the ^{119}Sn spectra from the binary series and the Na_2O ternary series. These show the typical lineshape for Sn(II) in the approximately axially symmetric environment created by sp^3 hybridization with the lone pair occupying one vertex

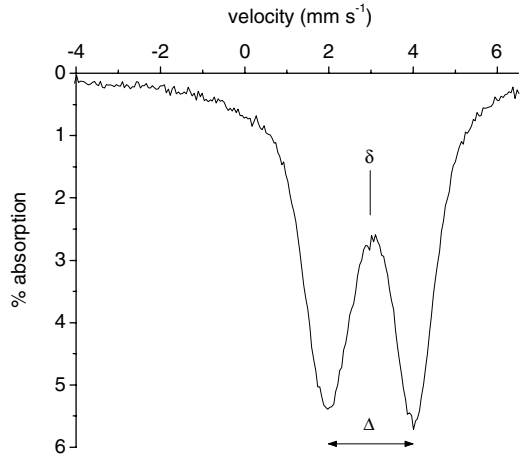

Figure 3. A typical ^{119}Sn Mössbauer spectrum showing the shift δ and quadrupole splitting Δ.

of the resulting pseudotetrahedron. The large linewidth reflects the chemical shift anisotropy (CSA) associated with the distortion. The peaks are fitted with CSA static lineshapes using the Winfit program [7] which yields values for the principal components of the chemical shift tensor (δ_{11}, δ_{22} and δ_{33}). The NMR lineshapes are more usually described in terms of three quantities derived from these principal components: the isotropic chemical shift $\delta_{\rm iso} = \frac{1}{3}(\delta_{11} + \delta_{22} + \delta_{33})$, which is influenced by the electron charge density in the surrounding bonds; the span $\Omega = (\delta_{11} - \delta_{33})$, which reflects the magnitude of the anisotropy and hence site distortion; and the skew $\kappa = \frac{3(\delta_{22} - \delta_{\rm iso})}{(\delta_{11} - \delta_{33})}$, which reflects the site symmetry. A typical fit to a binary spectrum is shown in figure 7(b) as the solid curve. The discrepancy in observed and fitted intensities could originate from a second site but it is more likely a reflection of the distribution of chemical shift anisotropy parameters of the single site. A single site simulation, even with added broadening, cannot accommodate these distributions, particularly the deviations away from axial symmetry.

The spectra from the ternary glasses show the emergence of a second peak which, from its position at ∼0 ppm and its narrow symmetric shape, arises from Sn(IV), tin in its higher oxidation state. The samples used for the ^{119}Sn NMR go to lower SnO (higher R_2O) concentrations than those used for ^{119}Sn Mössbauer [3] and the quantities of Sn(IV) only become significant at these lower concentrations. A typical fit to a ternary spectrum is shown in figure 8(b) where the Sn(IV) peak was treated as a Gaussian for fitting purposes. The Sn(II) parameters $\delta_{\rm iso}$, Ω and κ are plotted against SnO content for both binaries and ternaries in figure 9 and the relative amounts of Sn(II) and Sn(IV) in the ternary glasses are plotted as a function of *nominal* SnO content in figure 10.

4. Discussion

4.1. Compositional dependence of structural parameters

Figure 11 shows how the interatomic distances $R_{\rm Si-O}$ and $R_{\rm Sn-O}$ and the O–Sn–O bond angle obtained from neutron diffraction [1, 3] vary with replacement of SnO by R_2O in the glasses (the Si–O–Si bond angle shows no systematic change with composition). These data reflect the resilience of the [SnO_3] polyhedron in the binary system. Its geometry changes very little with composition (figures 11(b) and (c)) whereas there is significant change in the Si–O distance

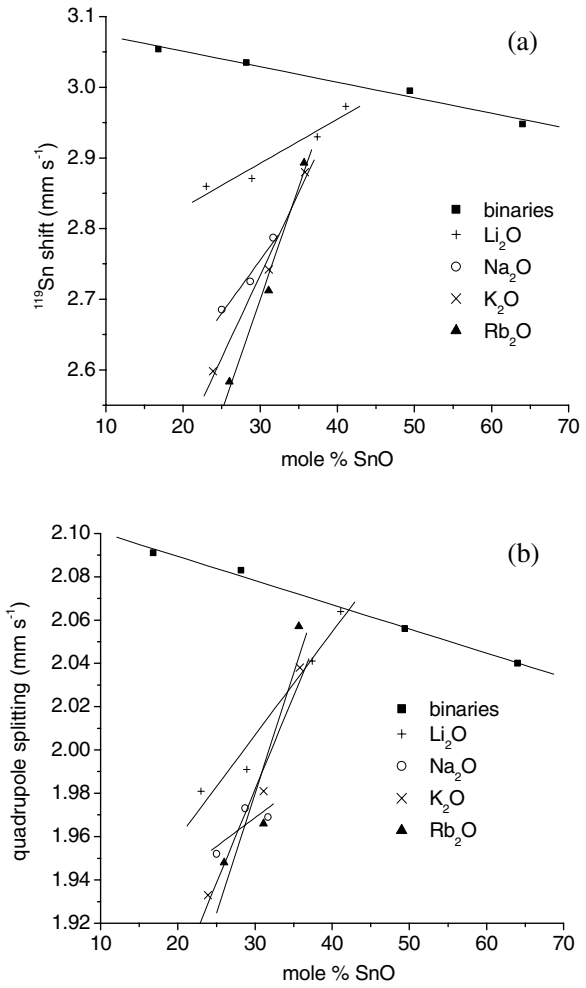

Figure 4. Variation in Mössbauer shift (a) and quadrupole splitting (b) with SnO content. Typical errors are ± 0.001 mm s^{-1}.

(figure 11(a)). However, in the ternary systems, when SnO is gradually replaced by R_2O, there is little change in R_{Si-O} and it is insensitive to the nature of the alkali cation R. It is the changes to the [SnO_3] polyhedron which become both more significant and alkali dependent. Nonetheless, the [SnO_3] unit is still retained and it is probably the medium-range organization of these units in the tetrahedral silicate network that gives rise to the intermediate-range features in the neutron diffraction distinct scattering plots. The distinctive alkali dependence of the O–Sn–O bond angle reflects the changes in molar volume (figure 1), i.e. Li^+ has little effect on the angle whereas the much larger Rb^+ increases the angle significantly.

In the binary system, a [SnO_3] polyhedron can only be accommodated in a tetrahedral network if one of the oxygen atoms in the polyhedron becomes 3-coordinate (i.e. Si_2OSn and eventually $SiOSn_2$). This factor is partly responsible for the rigidity of the [SnO_3] polyhedron. When R_2O is substituted for SnO, rather than the formation of Si–O^-R^+ non-bridging units, which would occur in an alkali silicate, the additional oxygen is used to reduce the coordination of the oxygen atoms in [SnO_3] by the formation of [$SnO_3^-R^+$] units in which all of the oxygen

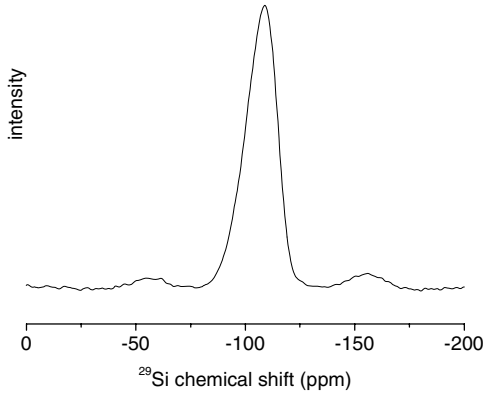

Figure 5. A typical ^{29}Si MAS NMR spectrum from a binary glass. Chemical shift is w.r.t. TMS.

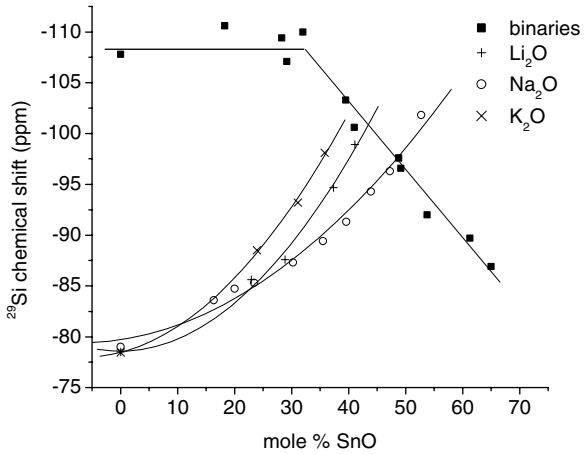

Figure 6. Variation of ^{29}Si chemical shift (w.r.t. TMS) with SnO content. Typical errors are ± 0.5 ppm.

atoms are 2-coordinate to silicon or other tin atoms. The change in connectivity, plus the presence of a nearby alkali ion, means that $[SnO_3]$ is affected more significantly than $[SiO_4]$. Such changes to polyhedral geometry should affect the symmetry and charge distribution at and near the various nuclei involved, either as a result of change in hybridization or of ionicity in the various bonds. These changes should be reflected in the ^{29}Si NMR and ^{119}Sn NMR and Mössbauer spectroscopy results.

4.2. Spectroscopic evidence

^{29}Si. Figure 12 shows how the ^{29}Si chemical shift changes with the various structural parameters $R_{Si–O}$, $R_{Sn–O}$ and O–Sn–O. Comparison of figures 12 and 11 shows that the ^{29}Si shift for the binary glasses increases with $R_{Si–O}$ and SnO concentration but is relatively insensitive to what is happening in the $[SnO_3]$ polyhedron. Conversely, the changes to the ^{29}Si shift in the ternaries are influenced more by what is happening in the $[SnO_3]$ polyhedron and are sensitive to the nature of the alkali cation R. These factors must influence the charge polarization in the Si–O bond.

If we assume a model where every SnO molecule produces one 3-coordinated oxygen but every R_2O molecule converts two 3-coordinated oxygens back to 2-coordinate, then we can

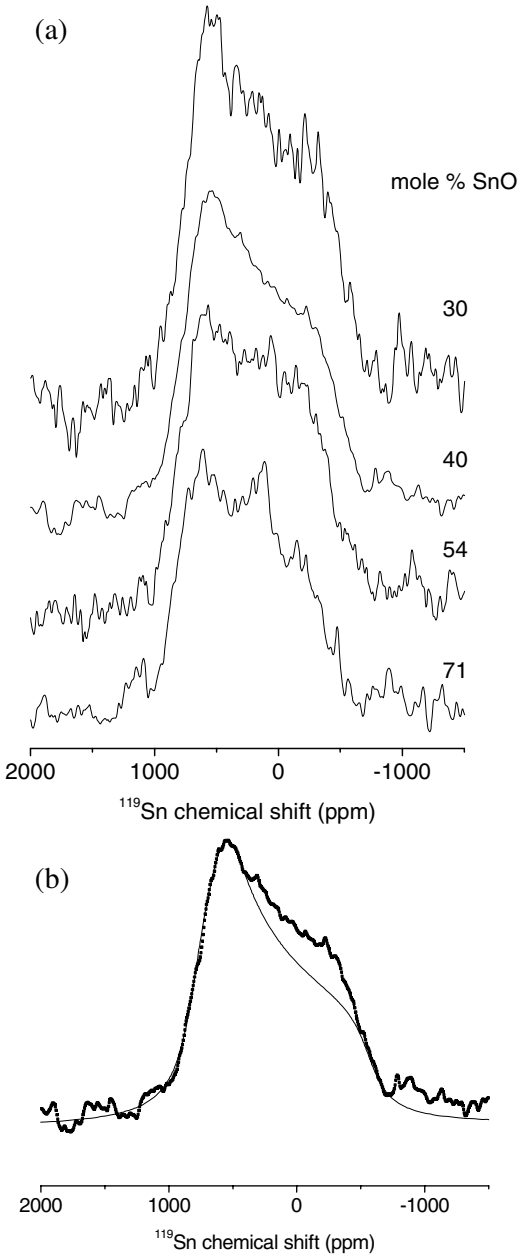

Figure 7. (a) ^{119}Sn static NMR spectra from the binary glasses. (b) A typical fit to a single CSA lineshape. The bold-dotted curve is the experimental spectrum and the continuous curve is the fit. Spectra are referenced to aqueous stannous chloride.

calculate an average oxygen coordination for each glass. Figure 14 shows the ^{29}Si chemical shifts for the glasses plotted against this average oxygen coordination and compared with data from the binary alkali silicates [9] in which the silicon environment can be described simply by the Q^n nomenclature, where n is the number of bridging oxygen atoms to silicon. Non-bridging oxygen atoms have a coordination of 1. The ^{29}Si chemical shifts in the ternary glasses

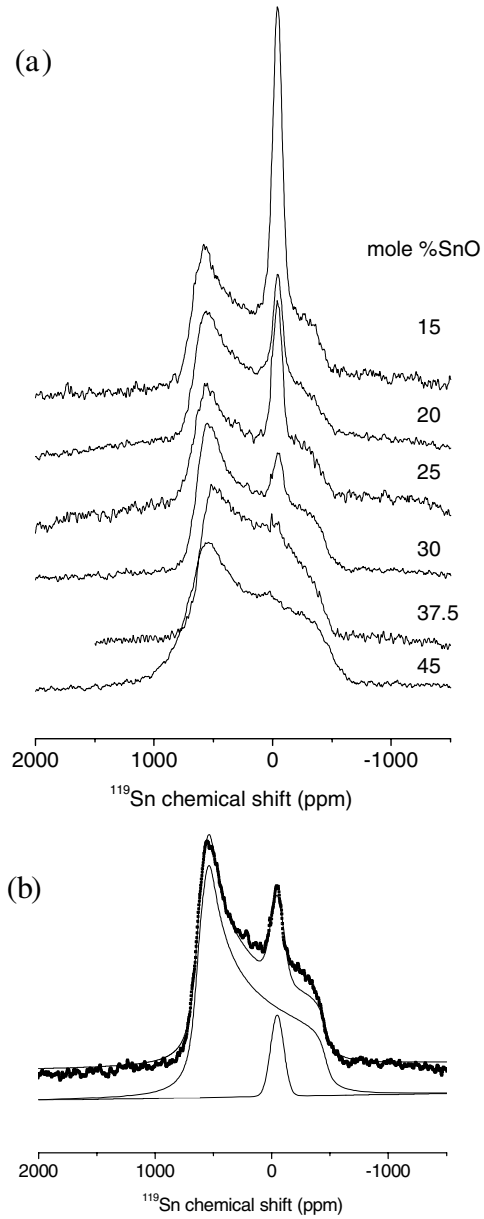

Figure 8. (a) ^{119}Sn static NMR spectra from the ternary glasses. (b) A typical fit with a single CSA lineshape plus a Gaussian. The bold-dotted curve is the experimental spectrum and the continuous curves are the total fit and the individual contributions. Spectra are referenced to aqueous stannous chloride.

are seen to fall on a continuous line which ultimately meets with the characteristic shift for a Q^2 species in the Na_2O–SiO_2 system. This figure illustrates the importance of charge distribution in bonds. When SnO is first added to SiO_2, there is almost no change in ^{29}Si chemical shift up to 30 mol% SnO, in spite of the different coordination polyhedron being inserted. This is due to the near identical electronegativities of Si and Sn. Beyond 30 mol% SnO, where there would be at least one 3-coordinated oxygen per silicon, the ^{29}Si shift starts to move to

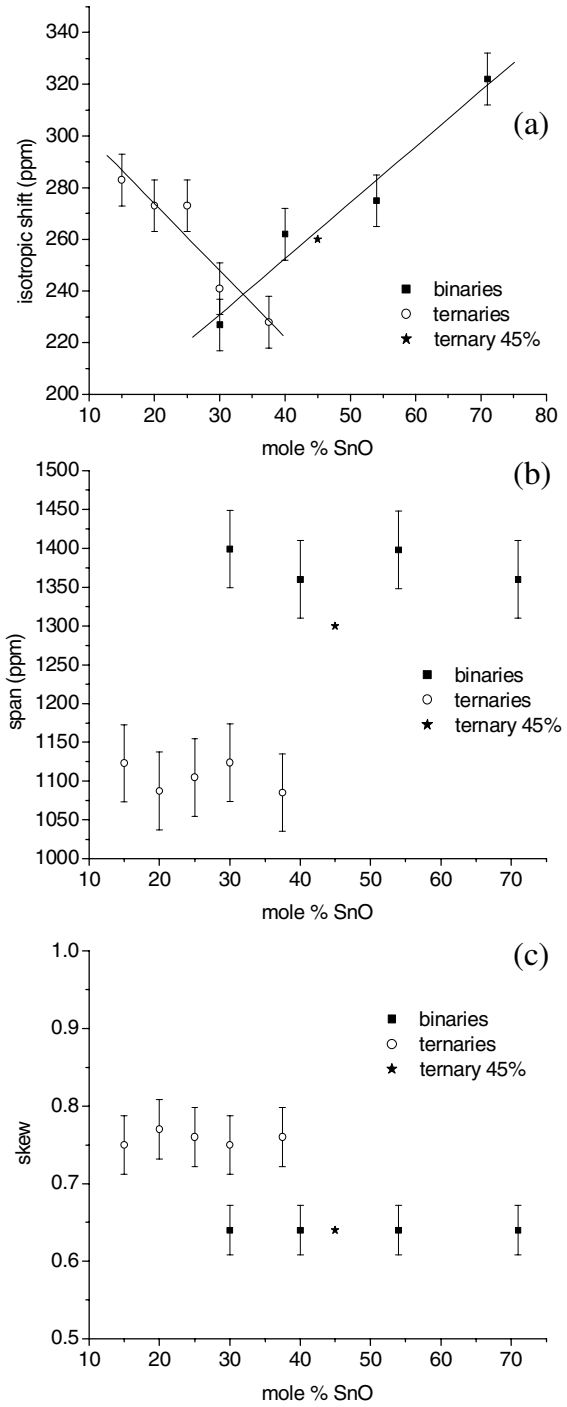

Figure 9. Variation in ^{119}Sn NMR parameters with SnO content for (a) isotropic shift, (b) span and (c) skew. The large errors reflect the strong interaction of these parameters with other fitting parameters such as line broadening.

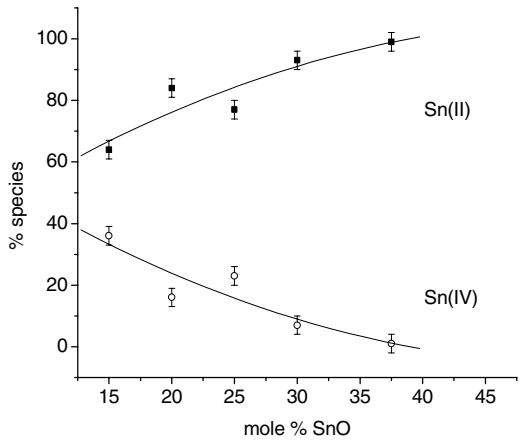

Figure 10. Change in the proportions of the Sn(II) and Sn(IV) species with SnO content in the Na_2O ternary glasses. Note that nominal compositions are used for this plot.

more positive values as the nucleus becomes more deshielded by the presence of the [SnO_3] units. When R_2O is substituted for SnO, the formation of [$SnO_3^-R^+$] units produces even greater deshielding and the eventual formation of Si–O^-R^+ non-bridging oxygens completes the transition to the alkali silicate behaviour.

^{119}*Sn–Mössbauer.* Figure 13 shows the dependence of ^{119}Sn Mössbauer shift on geometry [3]. Mössbauer shift reflects the s-electron density at the nucleus and the extent to which this is screened by the valence orbitals. This screening will be affected by both bond polarization and by changes in hybridization. The ^{119}Sn Mössbauer quadrupole splitting reflects the field symmetry at the nucleus which will depend on O–Sn–O bond angle (hybridization) and the equivalence of the nearest neighbour oxygens. The dependence of the quadrupole splitting on geometry (not shown) is very similar to that of the Mössbauer shift. Similar comments can be made to those in the preceding section about the different behaviour of the binary and ternary glasses.

^{119}*Sn NMR.* The spectrum shown in figure 8(b) was produced by Fourier transformation of an FID to which 4 kHz of line broadening had been applied to reduce noise. This broadens and distorts the line shape of the relatively narrow Sn(IV) resonance. Measurements taken from an unbroadened spectrum give a width for the Sn(IV) line of 7 kHz, compared to the 9 kHz typical of crystalline SnO_2 at this field. However, the unbroadened line shape remains symmetric, showing no singularities, unlike the axial pattern obtained from c-SnO_2. The main contribution to the width of the ^{119}Sn resonance from c-SnO_2 arises from the tetragonal distortion of the [SnO_6] polyhedron. We therefore conclude that the Sn(IV) cations in the glass are in a less distorted environment and the peak width is largely due to the distribution of bond lengths and angles which arise in an amorphous material. Thus the shape of the second ^{119}Sn peak in the ternary tin silicates confirms that this Sn(IV) is part of the glass structure and not in any crystal phase (in agreement with x-ray diffraction (XRD)). It has been observed that Sn(II) in glass can be oxidized to Sn(IV) by the process of grinding at room temperature or exposure of powder to atmosphere for long periods [8]. However, the ^{119}Sn NMR experiments were conducted on bulk samples whilst the x-ray diffraction, which was conducted on powder samples, showed no evidence of crystalline phases. If the

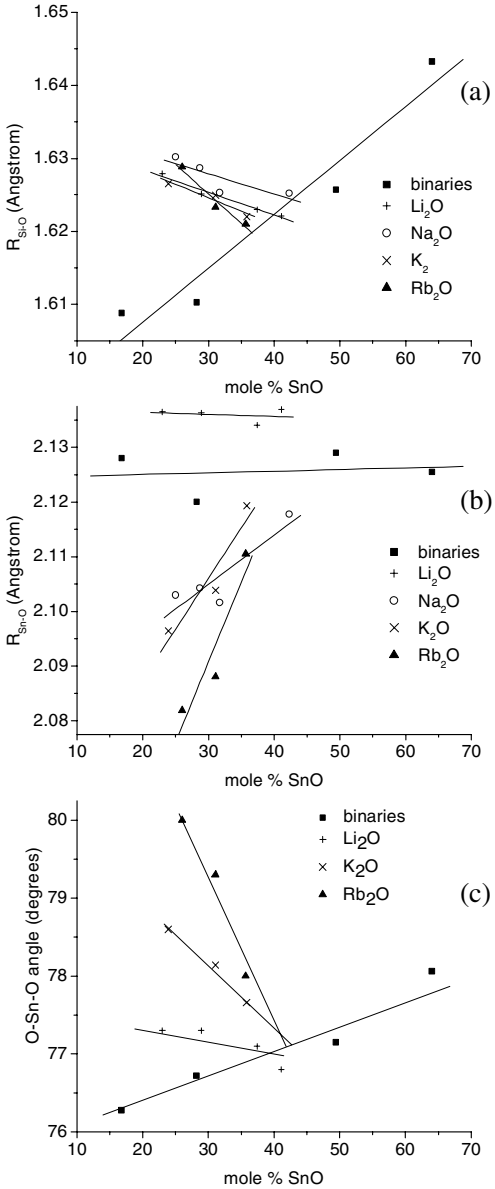

Figure 11. Change in polyhedron geometry with SnO content for (a) the Si–O distance $R_{Si–O}$, (b) the Sn–O distance $R_{Sn–O}$ and (c) the O–Sn–O bond angle. Typical errors are ±0.005 Å for the bond lengths and ±0.2° for the bond angles.

Sn(IV) were in a crystalline environment, the concentration is such (approximately equivalent to 7 mol% SnO_2 for the $x = 35$ sample) that peaks would be observable by XRD. The presence of Sn(IV) in sodium tin silicate glasses has been reported by Dannheim *et al* [10] who deliberately introduced SnO_2 into the glass batch and also changed the oxidation state by controlled atmosphere melting. They interpreted their Mössbauer results in terms of 4- and 6-coordinated sites for both Sn(II) and Sn(IV). The neutron diffraction information on the glasses studied here shows quite clearly that the Sn(II) coordination is 3 [1, 3]. We have no

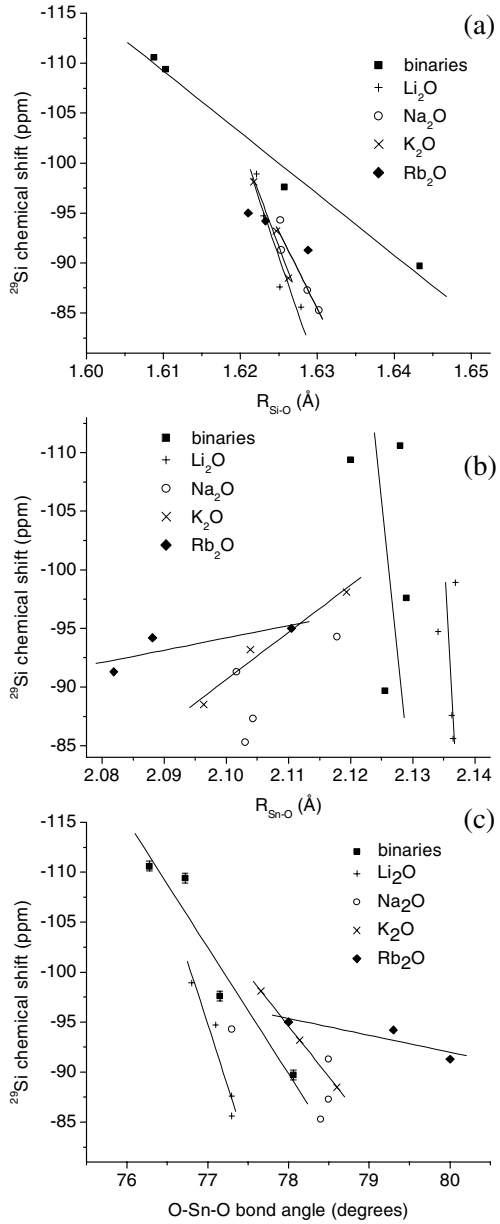

Figure 12. Variation in ^{29}Si chemical shift as a function of polyhedron geometry (a) the Si–O distance $R_{Si–O}$, (b) the Sn–O distance $R_{Sn–O}$ and (c) the O–Sn–O bond angle. Typical errors are ±0.5 ppm for the chemical shift, ±0.005 Å for the bond lengths and ±0.2° for the bond angles.

direct information on the Sn(IV) coordination though the symmetry might suggest [$Sn^{IV}O_4$] or [$Sn^{IV}O_6$] polyhedra with Na^+ for local charge balancing. However, the former would be expected to be at least 100 ppm to more negative shift values.

Figure 9 shows that the ^{119}Sn NMR spectra from the binary and ternary glasses have different values of span (figure 9(b)) and skew (figure 9(c)) which are almost independent

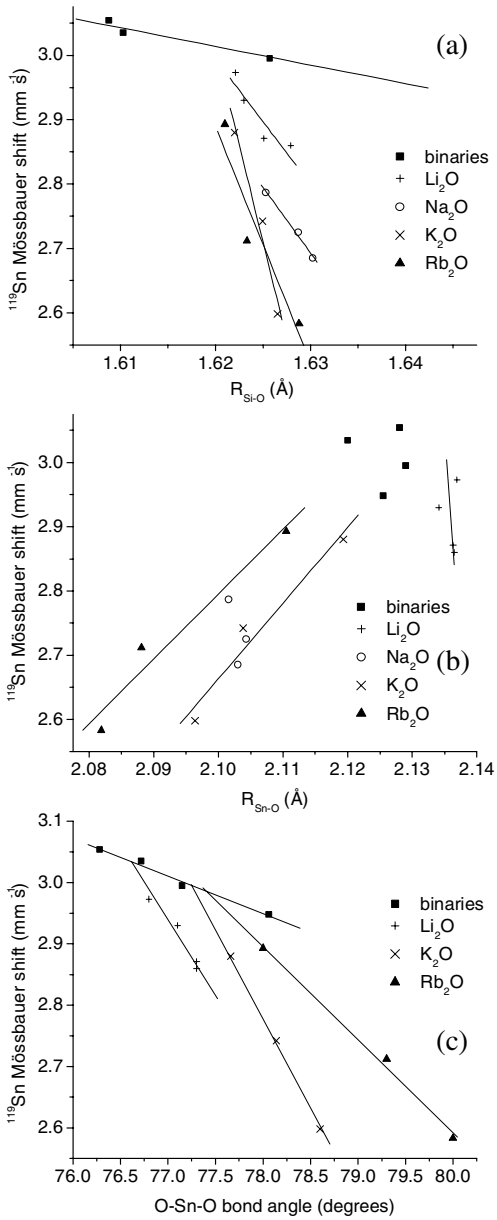

Figure 13. Variation in Mössbauer shift with polyhedron geometry (a) the Si–O distance R_{Si-O}, (b) the Sn–O distance R_{Sn-O} and (c) the O–Sn–O bond angle. Typical errors are ± 0.001 mm s^{-1}, ± 0.005 Å for the bond lengths and $\pm 0.2°$ for the bond angles.

of composition whilst their isotropic shifts show different dependences (figure 9(a)) on composition. The exception is the 45 mol% SnO sample from the ternary series which behaves more like a binary sample. This could represent a transition between the two types of behaviour or possibly the occurrence of phase separation into regions which are predominantly sodium silicate or tin silicate. The larger value of skew for the ternaries suggests that the environment is closer to axial than in the binaries because of the lower average oxygen coordination. Similarly,

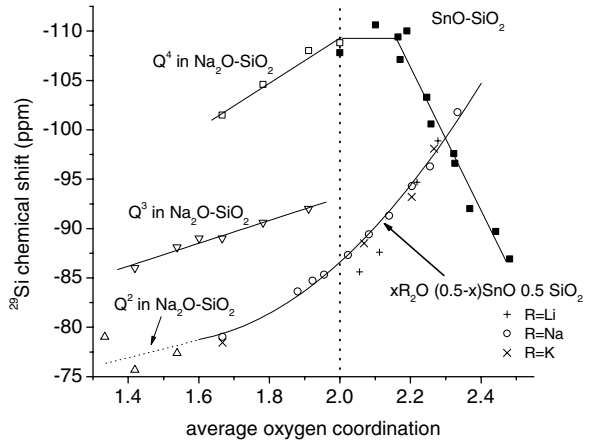

Figure 14. Change in ^{29}Si chemical shift (w.r.t. TMS) with average oxygen coordination compared with the shifts for the various Q species in binary sodium silicate glasses. Typical errors are ± 0.5 ppm.

the smaller value of span is consistent with lower oxygen connectivity reducing the distortion of the [SnO_3] polyhedron.

5. Conclusions

The environment of the Sn(II) species in oxide glasses is that of a well-defined trigonal pyramid with the lone pair of electrons forming a fourth vertex to give a pseudotetrahedral polyhedron. The symmetry of the charge distribution at the nucleus is less than axial because one or more of the oxygen atoms in the polyhedron are 3-coordinate rather than 2-coordinate, reducing the symmetry of the tin environment. Gradual substitution of R_2O for SnO reduces the oxygen coordination which then allows the [SnO_3] polyhedron to revert to a less strained condition. The presence of R^+ also stabilizes Sn(IV) in the glass matrix.

Acknowledgments

We thank the Engineering and Physical Sciences Research Council for funding of the NMR facility and Pilkington plc for chemical analysis. We also wish to thank all our colleagues who contributed to the earlier studies.

References

[1] Bent J F, Hannon A C, Holland D and Karim M M 1998 *J. Non-Cryst. Solids* **232–234** 300–8
[2] Williams K F E, Johnson C E, Johnson J A, Holland D and Karim M M 1995 *J. Phys.: Condens. Matter* **7** 9485–97
[3] Johnson J A, Johnson C E, Holland D, Sears A, Bent J F, Appleyard P, Thomas M F and Hannon A C 2000 *J. Phys.: Condens. Matter* **12** 213–30
[4] Sears A, Holland D and Dowsett M G 2000 *Phys. Chem. Glasses* **41** 42–8
[5] Keysselitz B and Kohlmeyer E J 1933 *Metall. Erz.* **30** 172
[6] Carbo-Nover J and Williamson J 1967 *Phys. Chem. Glasses* **8** 164–8
[7] Massiot D, Fayon F, Capron M, King I, Le Calvi S, Alonso B, Durand J-O, Bujoli B, Gan Z and Hoatson G 2002 *Magn. Reson. Chem.* **40** 70
[8] Appleyard P G 1999 *PhD Thesis* Liverpool John Moores University
[9] Dupree R, Holland D, McMillan P W and Pettifer R F 1984 *J. Non-Cryst. Solids* **68** 399
[10] Dannheim V H, Oel H J and Erlangen G T 1976 *Glastech. Ber.* **49** 170